High Performance Control for Induction Machines Based on Optimal Preview Control Technique

Mohamed M. Negm, Mohamed F. Salem, and Osama S. Ebrahim

***Abstract*—High performance induction motor (IM) drive system fed from space vector pulse width modulated (SVPWM) inverter and based on optimal preview control theory is realized. The synthesized control algorithm achieves motor speed control, constant flux control and field orientation control via an optimized control input command contains the synchronous angular speed and the two synchronously rotating components of the stator voltage vector. The novel error system used in building the optimal preview controller can cure the adverse phenomena caused by parameter uncertainty and unmodeled dynamics. With few feature values of the desired and disturbance signals the transient performance can be improved. A laboratory prototype was built and the overall control system is implemented using low cost multifunction data acquisition card (DAC). Where, the SVPWM switching patterns representing the control input command is realized by generating successive sector dependent digital words on DAC digital lines. Accordingly, the storage memory is minimized and the sawtooth carrier generator is eliminated. Extensive experimental results have been carried out to show the effectiveness and applicability of the proposed control system.**

***Index Terms*—Data acquisition card, optimal preview controller, induction motor, SVPWM.**

I. INTRODUCTION

SINCE 1980's, field oriented control (FOC) has been recognized as the algorithm which gives the induction motor (IM) drive the best dynamic performance. Most of FOC implementations are based on rotor flux orientation. However, this strategy is sensitive to both the rotor speed and rotor time constant which varies greatly with temperature, skin effect and, the flux saturation level in the iron core. Therefore, some errors can be expected in such scheme. To obtain a robust control, more sophisticated on line tuning methods were developed, which often adds to the complexity. On contrary, the stator quantities and parameters such as currents and resistance can be easily measured with good accuracy; therefore the stator flux can also be estimated more accurately than the rotor flux. Using the stator flux instead of the rotor flux as a feedback signal leads to implementation of stator flux oriented control which is more accurate and robust control [1]-[4]. In the stator flux oriented control, the stator leakage inductance is moved to the rotor side [1]. Accordingly, the stator flux response will follow immediately the input voltage command as long as the stator resistance voltage drop is small. Hence, voltage control is more preferred over the stator flux orientation. In today's industrial world pulse width modulated voltage source inverters (PWM-VSI) have been widely accepted because of existing low cost high performance switching power devices and needless to sophisticated feedback schemes which are mandatory employed to stabilize the motion of the IM driven by current source inverters (CSI). Different PWM techniques such as; sinusoidal PWM, hysteric PWM and the relatively new space vector pulse width modulation (SVPWM) technique, have been proposed [5]. The SVPWM technique is based on the space vector representation of the command voltage. In comparison with the sinusoidal PWM technique, the space vector PWM technique generates less harmonic distortion in the output voltages and currents, provides more efficient use for the DC bus voltage and requires less execution time and memory program for digital implementation [6], [7]. Advantages of the SVPWM such as; constant switching frequency, well defined harmonic spectrum, optimum switching pattern, minimization of switching losses and good utilization of the DC bus voltage cannot fed directly by classical current regulated PWM techniques [2], [7], [8]. Application of digital signal processor (DSP) to realize the SVPWM technique for 3-phase voltage source inverter has been proposed in [7], where an external sawtooth carrier generator is required.

Many applications of the modern control techniques for high performance control of the IM have been published, such as direct torque neruo-fuzzy control (DTNFC), neural network, adaptive neuro-fuzzy inference system (ANFIS). Further modern control includes variable structure control, adaptive control, and other optimal preview control are also proposed [2], [3], [9]-[12]. The advantages of optimal preview IM vector control such as; formal off line procedure to determine the controller gains, needless to tune these gains on line, optimality of the system performance, robustness against model mismatch, and improved stability are all declared [3], [6], [11].

In this paper, an optimal preview vector control for 3-phase IM fed from SVPWM inverter is realized using PC6014-NI low cost multifunction data acquisition card (DAC) [12]. The state equations of the IM suitable for voltage control are derived in a synchronously rotating reference frame using space vector method. The equations are then linearized about nominal operating point and the motor is described as 3-input, 3-ouput controlled object. The three input variables of this object are the synchronous angular speed and the two components of the stator voltage

Manuscript received July 12, 2004; revised April 4, 2005.

The authors are with the Department of Electrical Engineering, Ain-Shams University, Cairo, Egypt (e-mail: mmnegm@yahoo.com, o_shawky@yahoo.com).

Publisher Item Identifier S 1682-0053(05)0295

space vector and the three output variables are the rotor mechanical speed and the two components of the stator flux space vector. The objective of the synthesized controller is to achieve rotor speed control, constant flux control, and field orientation control. Novel error system is used to cope with the parameter variations and model mismatch. The preview controller is implemented with few future values of the desired and disturbance signals which represent the rotor speed and estimated load torque, respectively. The SVPWM technique is employed to realize the optimal control input signals. This is done by generating successive sector dependent digital words, representing the SVPWM switching patterns, on the DAC digital lines. Consequently, the storage area is minimized and the sawtooth carrier generator is eliminated.

II. Induction Motor Model

The dynamic equations of the three phase IM drive expressed in a coordinate system rotating at synchronous speed ($\alpha-\beta$ frame) is given by

$$\frac{d}{dt}\begin{bmatrix}\omega_r\\ \psi_{\alpha s}\\ \psi_{\beta s}\\ i_{\alpha s}\\ i_{\beta s}\end{bmatrix}=\begin{bmatrix}-\frac{F}{J}\omega_r+\frac{3P}{4J}(\psi_{\alpha s}i_{\beta s}-\psi_{\beta s}i_{\alpha s})-\frac{1}{J}T_L\\ \omega_e\psi_{\beta s}-R_s i_{\alpha s}+v_{\alpha s}\\ -\omega_e\psi_{\alpha s}-R_s i_{\beta s}+v_{\beta s}\\ \frac{\gamma_r}{\sigma L_s}\psi_{\alpha s}+\frac{\omega_r}{\sigma L_s}\psi_{\beta s}-\frac{(\gamma_s+\gamma_r)}{\sigma}i_{\alpha s}+\omega_s i_{\beta s}+\frac{1}{\sigma L_s}v_{\alpha s}\\ -\frac{\omega_r}{\sigma L_s}\psi_{\alpha s}+\frac{\gamma_r}{\sigma L_s}\psi_{\beta s}-\omega_s i_{\alpha s}-\frac{(\gamma_s+\gamma_r)}{\sigma}i_{\beta s}+\frac{1}{\sigma L_s}v_{\beta s}\end{bmatrix} \tag{1}$$

where $i_{\alpha s}, i_{\beta s}, \psi_{\alpha s}, \psi_{\beta s}, v_{\alpha s},$ and $v_{\beta s}$ are the $\alpha-\beta$ components of the stator current, flux linkage, and voltage space vector, respectively. The symbols $\omega_e, \omega_r,$ and ω_s denote the synchronous, rotor, and slip angular speed, respectively while, $P, T_L, F,$ and J are the total number of poles, load torque, equivalent mechanical friction and inertia constants, respectively. Further, L_m denotes the magnetizing inductance, while $L_s, R_s, L_r,$ and R_r are the stator and rotor self inductances and resistances, respectively. The coefficients $\gamma_s, \gamma_r,$ and σ are specified as

$$\gamma_s=\frac{R_s}{L_s},\quad \gamma_r=\frac{R_r}{L_r},\quad \sigma=1-\frac{L_m^2}{L_s L_r}. \tag{2}$$

The nonlinear IM model (1), expressed in terms of state space notation as

$$\dot{x}(t)=f(x(t),u(t),d(t)) \tag{3}$$

where the state variable $x(t)$, the input variable $u(t)$, and the disturbance signal $d(t)$, are given by

$$\begin{aligned}x(t)&=[\omega_r \quad \psi_{\alpha s} \quad \psi_{\beta s} \quad i_{\alpha s} \quad i_{\beta s}]^t\\ u(t)&=[\omega_e \quad v_{\alpha s} \quad v_{\beta s}]\\ d(t)&=T_L\end{aligned} \tag{4}$$

the superscript " t " denotes matrix transposing.

III. Optimal Preview Controller

Linearizing (1) around nominal operating point (x_0,u_0,d_0) by the small signal approximation technique yields

$$\begin{aligned}\dot{x}(t)&=A_0x(t)+B_0u(t)+C_0d(t)\\ y(t)&=Ex(t)=[\omega_r \quad \psi_{\alpha s} \quad \psi_{\beta s}]^t\end{aligned}. \tag{5}$$

The constant matrices $A_0, B_0, C_0,$ and E_0 are given by

$$\begin{aligned}A_0&=\left.\frac{\partial f(.)}{\partial x}\right|_{(x_0,u_0,d_0)},\quad B_0=\left.\frac{\partial f(.)}{\partial u}\right|_{(x_0,u_0,d_0)},\\ C_0&=\left.\frac{\partial f(.)}{\partial d}\right|_{(x_0,u_0,d_0)},\quad E_0=\begin{bmatrix}1&0&0&0&0\\0&1&0&0&0\\0&0&1&0&0\end{bmatrix}.\end{aligned} \tag{6}$$

The discrete time equivalent of (5) is given by

$$\begin{aligned}x(k+1)&=Ax(k)+Bu(k-1)+Cd(k)\\ y(k)&=Ex(k)\end{aligned}. \tag{7}$$

where the input vector $u(k)$ is delayed by one sampling period to compensate for the microprocessor execution time. Define the error signal $e(k)$ as the difference between the desired variable $R(k)$ and the output variable $y(k)$,

$$e(k)=R(k)-y(k). \tag{8}$$

An error system can be constructed from (7) and (8)

$$X(k+1)=\Phi X(k)+\Gamma\Delta u(k)+G_r\Delta Z(k)+G_d\Delta d(k) \tag{9}$$

where Δ is the first difference operator and

$$\Phi=\begin{bmatrix}I_3&I_3&0&0\\0&I_3&E(I_5-A)&-EB\\0&0&A&B\\0&0&0&0\end{bmatrix},\quad \Gamma=\begin{bmatrix}0\\0\\0\\I_3\end{bmatrix}$$

$$G_r=\begin{bmatrix}0\\I_3\\0\\0\end{bmatrix},\ G_d=\begin{bmatrix}0\\-EC\\C\\0\end{bmatrix},\ X(k+1)=\begin{bmatrix}e(k)\\\Delta e(k+1)\\\Delta x(k+1)\\\Delta u(k)\end{bmatrix}. \tag{10}$$

$$\Delta Z(k+1)=\Delta R(k+1)-\Delta R(k)$$

The performance index J_d is selected as

$$J_d=\sum_{j=0}^{\infty}X(j+1)^tQX(j+1)+\Delta u(j)^tR\Delta u(j) \tag{11}$$

Minimization of the performance index in (11) subject to the constraints in (7) leads to the following real time optimal preview control law as in [3], [6], [10]

$$\begin{aligned}u(k)=g_1\sum_{i=0}^{k}e(i)+(g_2-g_1)e(k)+g_3x(k)+\\ g_4u(k-1)+\sum_{j=1}^{M}\{F_{rj}[\Delta R(k+j)-\Delta R(j)]\\ +F_{dj}[\Delta d(k+j-1)-\Delta d(j-1)]\}\end{aligned} \tag{12}$$

where $G=[g_1 \ g_2 \ g_3 \ g_4]$

$$F_{rj}=G_jG_r,\ F_{dj}=G_jG_d,\ \text{for}\ j=1,2,\ldots,M$$

Feedback gain: $G=-\gamma\Gamma^tK\phi$

Feedforward gain: $G_1=-\gamma\Gamma^tK$, $G_2=-\gamma\Gamma^t\phi^t\lambda$,

$G_j=G_{j-1}K_1$, for $j=3,4,\ldots,M$

$K_1=K^{-1}\phi^t\lambda$ where K,γ and λ are the steady state solution of the following algebraic Riccati's equation

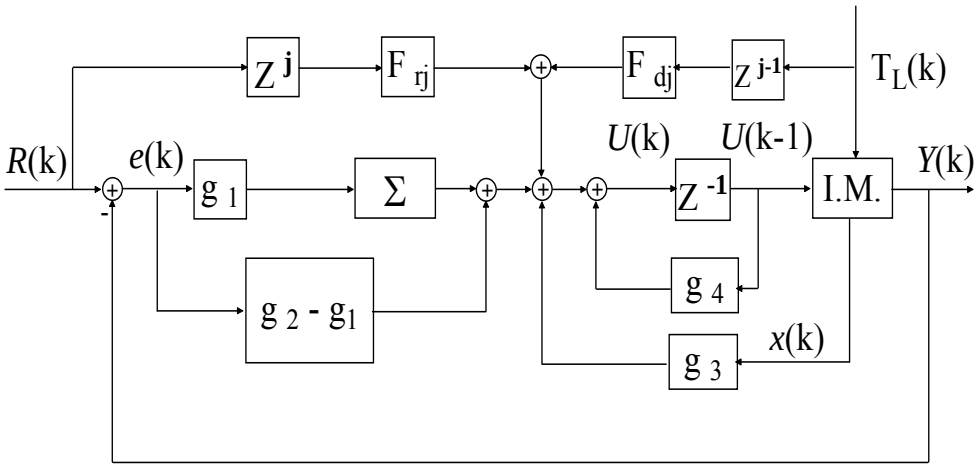

Fig. 1. Optimal preview controller structure.

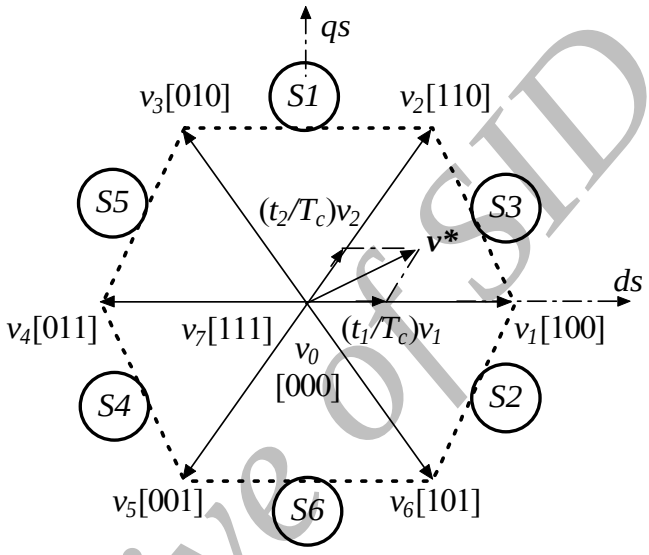

Fig. 2. SVPWM basic space vectors and sectors.

$$K(i) = Q + \Phi^t \lambda(i+1)\Phi$$
$$\lambda(i+1) = K(i+1)[I_{14} - \Gamma\gamma(i+1)\Gamma^t K(i+1)]. \qquad (14)$$
$$\gamma(i+1) = [R + \Gamma^t K(i+1)\Gamma]^{-1}$$

The weighting matrices of the error and input signals in performance index (11) have the following structure

$$Q = \begin{bmatrix} q & q & 0 \\ q & q & 0 \\ 0 & 0 & 0 \end{bmatrix} (14\times 14),\ R = r$$
$$q = \begin{bmatrix} q_1 & 0 & 0 \\ 0 & q_2 & 0 \\ 0 & 0 & q_3 \end{bmatrix},\ R = \begin{bmatrix} r_1 & 0 & 0 \\ 0 & r_2 & 0 \\ 0 & 0 & r_3 \end{bmatrix}. \qquad (15)$$

All the parameters of the optimal preview control law are defined straight forward and implemented as indicated in Fig. 1. The symbol M denotes the preview steps.

IV. SVPWM Implementation

Fig. 2 shows the six sectors limited by eight discrete vectors, in the stationary reference frame (d-q frame), which are corresponding to the possible combinations of ON and OFF states of the power transistors in two levels three phase inverter. The length of the nonzero vectors is two thirds of the DC bus voltage while the angle between any two adjacent non-zero vectors is 60 degrees. The zero vectors are at the origin and apply zero voltage to a three phase loads. The eight vectors are called the basic space vectors and are denoted by $v_0 = [0\,0\,0]$, $v_1 = [1\,0\,0]$, …, $v_7 = [1\,1\,1]$. The objective of the SVPWM technique is to instantaneously realize the reference voltage v^*, by controlling the duration of the switching states corresponding to the basic space vectors such that in one switching period, the average output voltage can be written as

$$v^*(t) = \frac{t_0}{T_c}v_0 + \frac{t_1}{T_c}v_1 + \ldots\frac{t_7}{T_c}v_7. \qquad (16)$$

where $t_0, t_1, \ldots, t_7$ are the turn ON time of the vectors $v_0, v_1, \ldots, v_7$; $\sum t_i \le T_c$ and T_c is the switching period. The decomposition of v^* into $v_0, v_1, \ldots, v_7$ has infinite ways.

However, in order to reduce the switching actions and make full use of active turn-on time of the space vectors, the reference voltage is normally split into two nearest adjacent voltage vectors and two zero-vectors v_0 and v_7 in an arbitrary sector. For example, in sector 3, in one switching period, the reference voltage can be expressed as

$$v^*(t) = \frac{t_0}{T_c}v_0 + \frac{t_1}{T_c}v_1 + \frac{t_2}{T_c}v_2 + \frac{t_7}{T_c}v_7. \qquad (17)$$

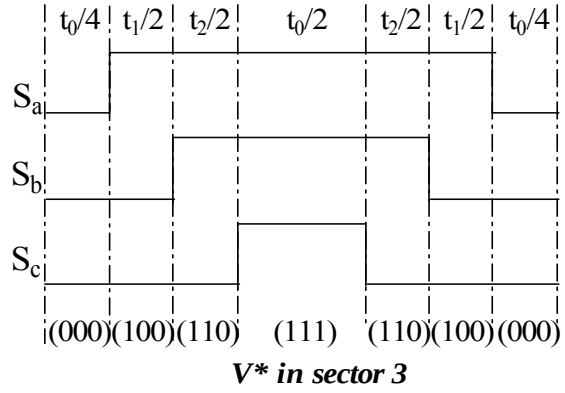

Fig. 3. Sector -3, PWM switching patterns.

Symmetrical SVPWM implies that

$$t_0 = t_7 = 0.5(T_c - t_1 - t_2)\,. \tag{18}$$

The following steps will indicate the on-line implementation of the proposed symmetrical regular sampling SVPWM algorithm.

Step 1: is to know which sector the reference vector v^*, defined by v_{ds} and v_{qs}, is in. The following three tests give the sector number as an output [5], [7]

$$\begin{aligned} tst_1 &= v_{qs}^* \\ tst_2 &= v_{ds}^* \sin 60^\circ - v_{qs}^* \sin 30^\circ \\ tst_3 &= -v_{ds}^* \sin 60^\circ - v_{qs}^* \sin 30^\circ \\ SectorNum &= sig(tst_1) + 2sig(tst_2) + 4sig(tst_3) \end{aligned} \tag{19}$$

where

$$\begin{aligned} sig(tst_i) &= 1 \ \text{ if } \ tst_i > 0 \\ sig(tst_i) &= 0 \ \text{ if } \ tst_i \le 0 \end{aligned} \qquad i = 1,2,3\,.$$

Step 2: is to calculate and saturate the duration of the two-sector boundary vectors t_1 and t_2 based on the sector number as follows:

Let,

$$\begin{aligned} K &= \frac{T_c}{V_{dc}}(\sqrt{3}v_{qs}^*) \\ L &= \frac{T_c}{V_{dc}}(\frac{\sqrt{3}}{2}v_{qs}^* + \frac{3}{2}v_{ds}^*) \\ M &= \frac{T_c}{V_{dc}}(\frac{\sqrt{3}}{2}v_{qs}^* - \frac{3}{2}v_{ds}^*) \end{aligned} \tag{20}$$

such that the duration periods are given in Table I.

The saturated duration periods t_{1sat} and t_{2sat} are illustrated as follows

$$\text{If } \ (t_1 + t_2) > T_c \ \text{ Then } \quad \begin{aligned} t_{1sat} &= t_1 T_c / (t_1 + t_2) \\ t_{2sat} &= t_2 T_c / (t_1 + t_2) \end{aligned} \tag{21}$$

Step 3: is to determine the proper switching patterns to be generated according to the sector number.

Fig. 3 shows switching waveforms of a symmetric switching scheme for a reference voltage lies in sector 3. The scheme can be easily implemented with the DAC by using successive sector dependent digital words to be generated on its digital lines. Table II gives the digital words represented in binary notation according to the sector number.

TABLE I
DURATION PERIODS t_0 AND t_1

Sector	1	2	3	4	5	6
t_1	M	L	$-M$	$-K$	K	$-L$
t_2	L	$-K$	K	M	$-L$	$-M$

TABLE II
SECTOR DEPENDENT DIGITAL WORDS

Sector	1	2	3	4	5	6
DW0	(000)	(000)	(000)	(000)	(000)	(000)
DW1	(010)	(100)	(100)	(001)	(010)	(001)
DW2	(110)	(101)	(110)	(011)	(011)	(101)
DW3	(111)	(111)	(111)	(111)	(111)	(111)

Step 4: is to calculate the necessary delay times for each digital word to be resident on the digital lines of the converter card as

$$\begin{aligned} Delay_0 &= 0.25t_0, \ Delay_1 = 0.25t_1 \\ Delay_2 &= 0.25t_2, \ Delay_3 = 0.25t_0 \end{aligned}\,. \tag{22}$$

Step 5: is to generate the proper sequence of the digital words with duration periods controlled by (21) using the following software commands:

```
DIG_Out_Prt (DWj)
    NIDAQDelay (Delayj)
```
(23)

for $j = 0,\ 1,\ 2$, and 3, and then repeat in reverse order. Where, DIG_Out_Prt (.) represents a digital output routine called from C++ programming environment, while NIDAQDelay (.) represents a stalling dummy loop whose time period determined by the augmented value [13].

V. STATOR FLUX ESTIMATOR

The stator flux space vector in the stationary reference frame (d-q frame) can be estimated from the space vectors of the stator voltage and current as

$$\hat{\psi}_s = \frac{v_s - R_s i_s}{s}, \quad s = \frac{d}{dt}\,. \tag{24}$$

The integration drift problem due to the dc offset and measurement noise can be avoided by using high pass filter, hence (23) becomes

$$\hat{\psi}_s = \frac{v_s - R_s i_s}{s + \omega_c}\,. \tag{25}$$

The cut-off frequency ω_c is selected fairly small compared to the working frequency to reduce the phase and magnitude errors. In this work, the fundamental component of the stator voltage provided by the inverter is assumed to be equal to the reference voltage. The errors caused by this assumption are often small in medium and high speed ranges. While at low speeds, the errors caused due to voltage drops and dead times in the switching devices become more prominent in the output voltage. Further, precise results can be achieved by using an inverter modulator as proposed in [4], [6].

VI. COORDINATE TRANSFORMATION

The coordinate transformation angle, θ, is generated from the command synchronous speed ω_e^*, output from the controller as follows

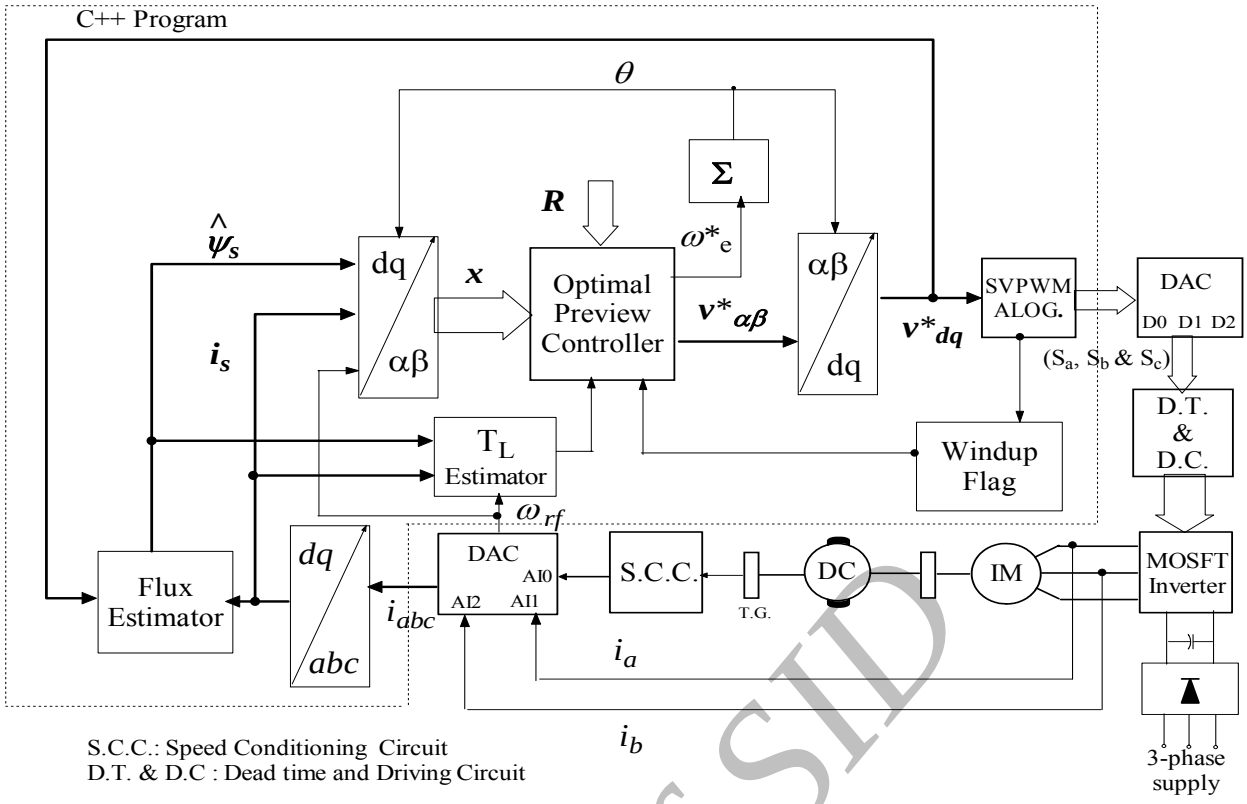

Fig. 4. Experimental system layout.

$$\theta(t) = \int \omega_e^*(t)dt \tag{26}$$

with an initial value equal zero.

VII. Load Torque Estimator

The load torque which represents the disturbance signal in the optimal control law (12) is estimated from the electromagnetic torque, T_{em}, as

$$\hat{T}_L = T_{em} - Js\omega_\gamma - F\omega_\gamma \tag{27}$$

where,

$$T_{em} = \frac{3}{4}P(\psi_{\alpha s}i_{\beta s} - \psi_{\beta s}i_{\alpha s}) . \tag{28}$$

A suitable variable gain digital filter is employed at the output stage of the load torque estimator to attenuate the wide frequency range noise with minimal delay [14].

VIII. Experimental System Layout

Fig. 4 shows the IM drive system schematic diagram based on the proposed optimal preview controller. In this figure all blocks inside the dotted line box represent software programming functions written in C++ and executed on Pentium-III- personal computer with 750 MHz clock and 250 MB RAM. Euler's backward method is used to map (24), (25) and (26) into the discrete form. Some hardware blocks in the schematic can be realized by using application specific IC (ASIC) to give more compact packing and enhanced performance. However for the stage of prototype verification it was decided to avoid the cost associated with such approach and the design is tuned toward the use of discrete and commercially available components in the Egyptian market. The IM considered is 4-pole, 1 kW, 130 V, 50 Hz, star connected with the following parameters: $J = 0.02$ N.m.s^2; $F = 0.0035$ N.m.s, $R_s = 0.89\,\Omega$; $L_s = 0.11$ H; $R_r = 0.92\,\Omega$; L_r = 0.11 H and L_r = 0.1 H, and loaded with 0.72 kW separately excited DC generator.

Two current sensors (LEM LTS 25-NP) are used to convert the stator phase currents i_a and i_b to a proper voltage signals. The tacho-generator speed signal is filtered and reduced to suitable level through a speed conditioning circuit block. To avoid controller windup, an anti-windup flag is activated when the inverter is being saturated and this in turn will stop updating the integral part of the optimal control low till normal operation retained again. This was necessary to mitigate the noise and improve performance. The stator voltages command are transformed to the stationary frame and processed through the SVPWM algorithm where 1.25 kHz switching frequency is used. The switching patterns are generated on the digital lines (D0, D1 and D2) of the DAC with a duration controlled by the computed switching intervals as explained in Section IV. The generated PWM switching signals are then fed to a dead time circuit, where the 3-PWM signals are complemented to get 6-PWM signals and a proper blanking time of 40 μs is provided for the high and low side signals of the same phase. The outputs of the dead time circuit are then isolated and amplified in the driver circuit to provide adequate PWM gating signals for the 3-phase MOSFET inverter circuit. A DC bus voltage of 190 V is obtained by 3-phase diode bridge rectifier and filtered with a 2000 μF capacitor filter such that it could be considered constant. The time required to perform the necessary calculations and data storage is found to be 0.4 ms, therefore 1.2 ms sampling period is selected.

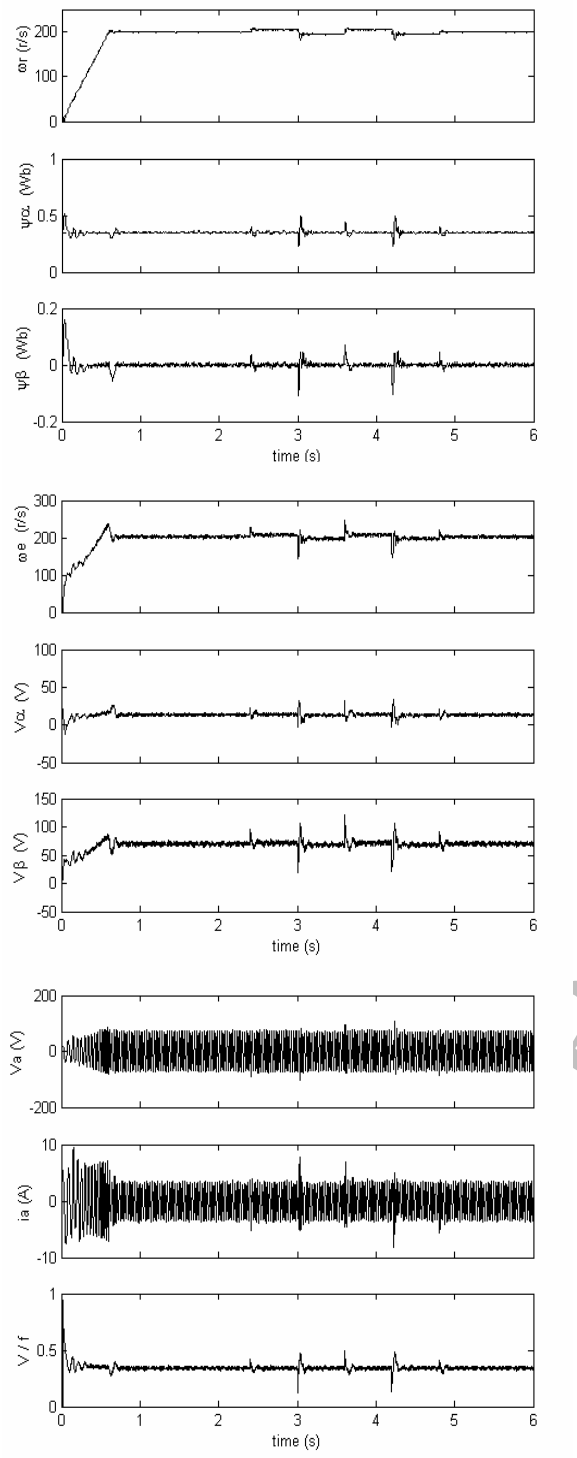

Fig. 5. Experimental response of the drive system.

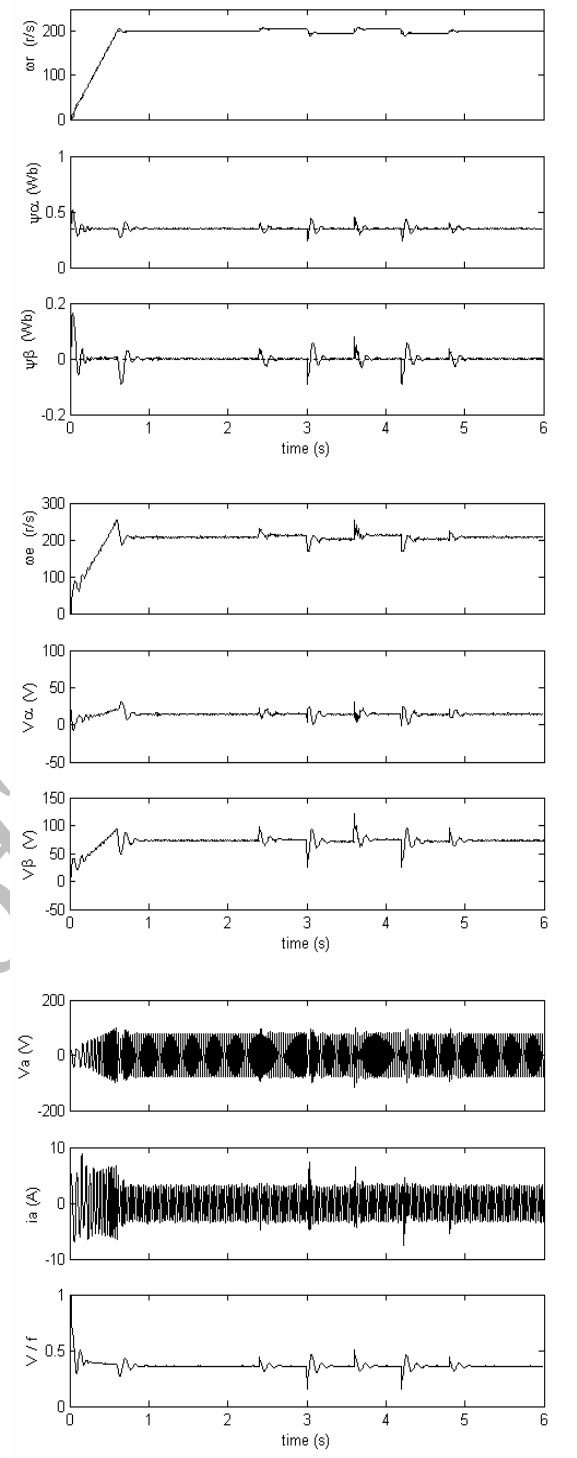

Fig. 6. Simulated response of the drive system.

IX. Experimental Results

In order to achieve constant flux control and field orientation control, the desired two components of the stator flux vector are chosen to be $\psi_{as}^{d} = 0.35$ Wb and $\psi_{bs}^{d} = 0.0$ Wb, respectively. In Figs. 5 to 10, the horizontal lines denote the time in second furthermore, the desired values of the rotor speed and the two components of the stator flux are illustrated by dotted lines while their response (ω_r, ψ_{as} and, $\psi_{\beta s}$) and the command input variables (ω_e^*, v_{as}^* and, $v_{\beta s}^*$) are demonstrated by solid lines. The weighting factors are chosen to be $q_1 = 10,\ q_2 = q_3 = 2000,\ r_1 = r_2 = r_3 = 10.$

A Matlab® simulation program is constructed to simulate the drive system. Where, the nonlinear IM dynamic model is solved using Runge-Kutta 4th order method. Further, the inverter switching patterns are simulated by 70 points to emulate a digital transfer rate of 70 kword/s of the DAC. The dead time effect on the inverter output voltage is neglected.

First the desired speed is ramped from 0 to 200 r/s in 0.6 s while the motor operates under a linear increasing load up to 25 % of rated torque. The desired speed is then changed abruptly with 10 r/s peak to peak during steady state conditions. Figs. 5 and 6 show the corresponding experimental and simulated results, respectively with good agreement. The vertical lines depict from up to down

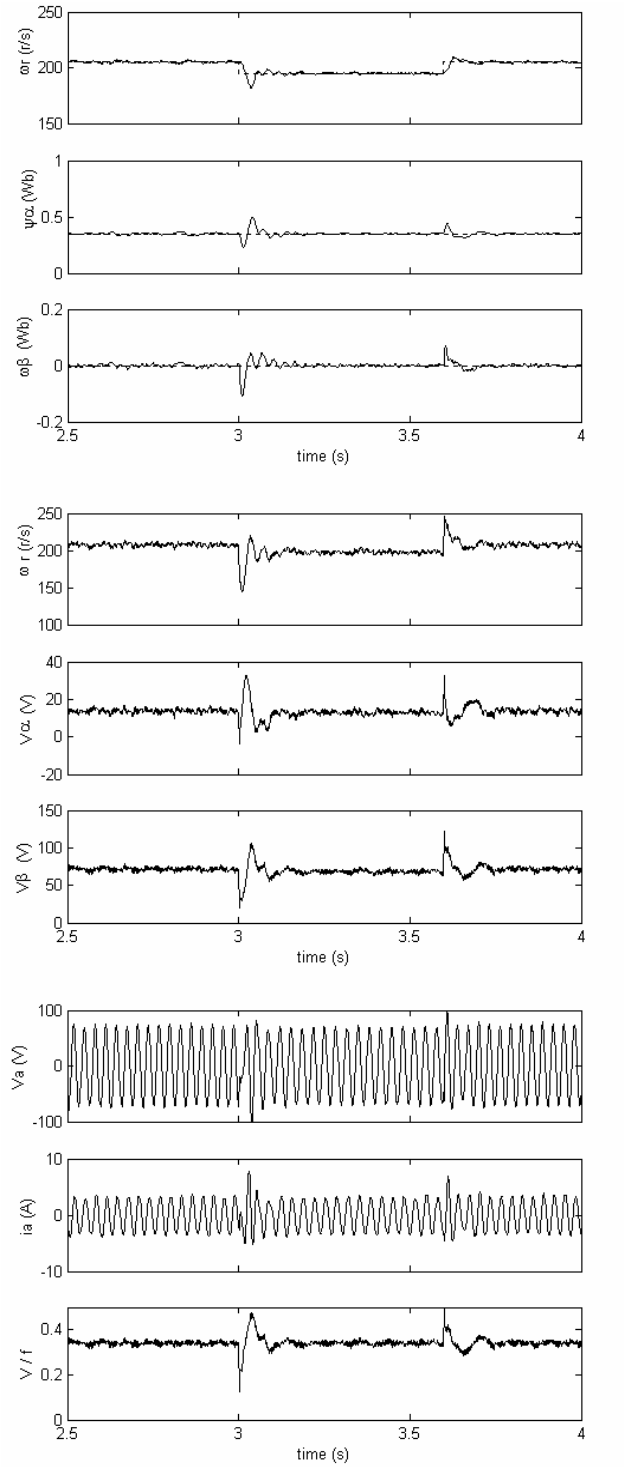

Fig. 7. An enlarged part of Fig. 5.

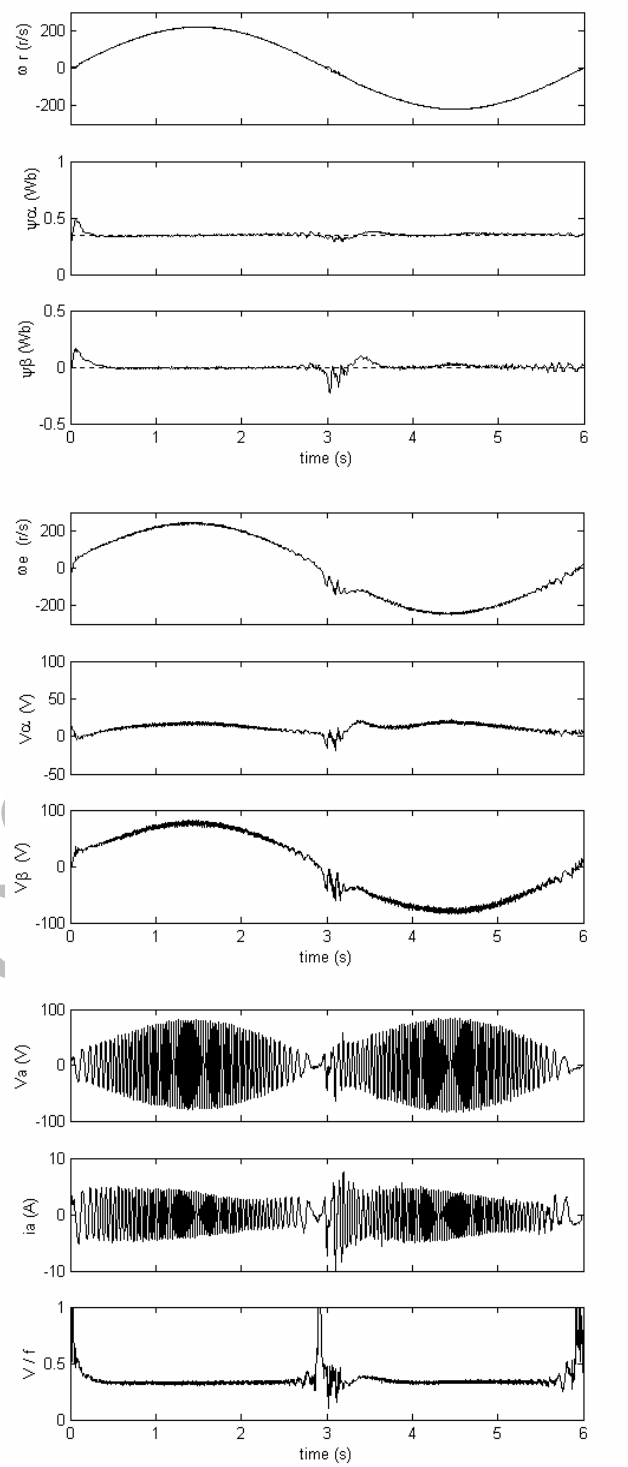

Fig. 8. Drive response for sinusoidal speed command.

rotor speed in r/s, α -component of the stator flux vector in Wb, β -component of the stator flux vector in Wb, synchronous speed command in electrical radian per second (r/s), α -component of the stator voltage vector command in V, β-component of the stator voltage command in V, voltage of phase a in V, current of phase a in A, and, computed voltage to frequency ratio, respectively. Fig. 7 is an enlarged part of Fig. 5 during the abrupt change in the speed command. The constant voltage to frequency ratio is inherently satisfied with trivial variations during transient states. Fig. 8 demonstrates the ability of the drive system to track wide variation in the desired speed where, a sinusoidal speed command of 440 r/s peak to peak is traced. Fig. 9 shows the effect of changing the preview steps $(M = 0, 2)$ on the transient response of the drive when the speed command is changed from 125 r/s to 135 r/s abruptly. Fig. 10 shows the ability of the proposed control scheme to attenuate the effects of sudden load torque variations from 25 % to 50 % abruptly with $M = 1$.

X. CONCLUSION

An optimal preview vector control of IM drive is realized in this paper. The experimental results obtained show the applicability and effectiveness of the proposed control scheme to achieve speed control, constant flux control and field orientation control over wide speed control range. From the test results have been carried out,

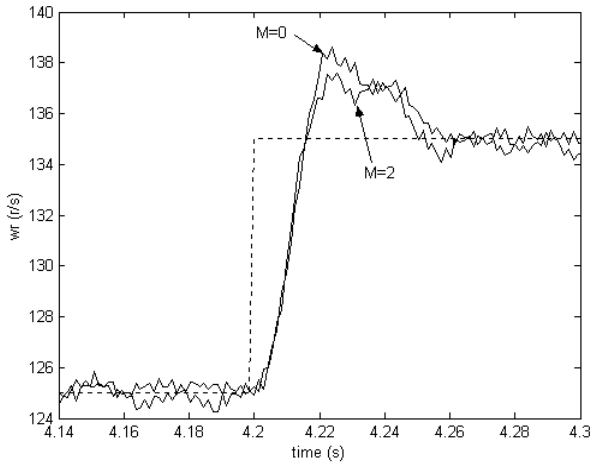

Fig. 9. Effect of changing the preview steps ($M = 0, 2$).

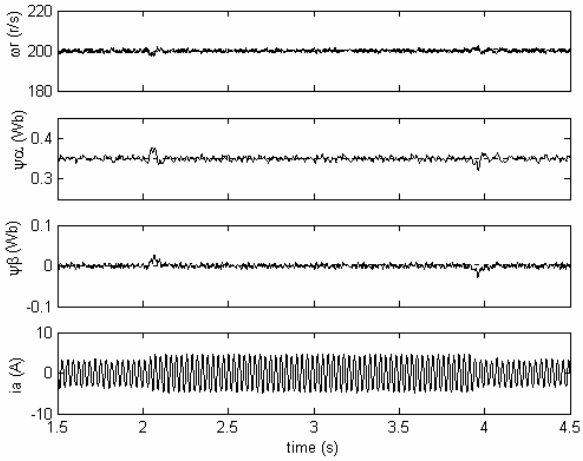

Fig. 10. Effect of changing the load torque abruptly.

the following important features are concluded: 1) formal and easy procedure to obtain the off line controller gains, 2) needless to tune the controller gains on line, 3) suitability for on line implantation owing to simplicity of the control law structure, 4) good robustness against un-modeled dynamics and parameter variations, 5) ability to use few preview steps to improve the transient response whenever it was needed, 6) good performance during sudden change in the speed command and/or load torque which may be desirable in many applications. As a further development, implementation of this control scheme in sensorless IM drive is currently in progress.

REFERENCES

[1] D. W. Novotny and T. A. Lipo, *Vector Control and Dynamics of AC Drives*, Oxford University Press Inc., Third Edition, 1997.

[2] Y. S. Lai and J. H. Chen, "A new approach to direct torque control of induction motor drive for constant inverter switching frequency and torque ripple reduction," *IEEE Trans. On Energy Conversion*, vol. 16, no. 3, pp. 220-227, Sep. 2001.

[3] M. M. Negm, S. A. Leithy, S. A. Dora, and H. A. Kamel, "Application of optimal preview controller for speed control of induction motor," in *Proc. Of AUPEC'98*, vol. 1, pp. 118-124, Australia, 1998.

[4] J. Holtz and J. Quan, "Sensorless vector control of induction motors at very low speed using nonlinear inverter model and parameter identification," IEEE *Transactions on Industry Applications*, vol. 38, no. 4, pp. 1087-1095, Jul./Aug. 2002.

[5] M. P. Kazmierkowski, "Control strategies for PWM rectifier/inverter fed induction motors," in *Proc. of IEEE Int. Symp. on Industrial Electronics, ISIE2000*, vol. 1, pp. TU15- TU23, Mexico, 2000.

[6] O. S. Ebrahim, M. F. Salem, and M. M. Negm, "Realization of optimal preview controller for high performance control of three phase induction machines," in *Proc. 9th Int. Middle East Power Systems*, MEPCON'2003, pp. 323-330, Menofiya University, Egypt, 2003.

[7] Texas Instrument, *Space Vector PWM with TMS320C24x/F24x Using Hardware and Software Determined Switching Patterns*, Application Report: SPRA524, 1999.

[8] M. P. Kazmierkowski and L. Maslesani, "Current control techniques for three phase voltage source PWM converters: A survey," *IEEE Trans. Ind. Elec.*, vol. 45, no. 5, pp. 691-703, Oct. 1998.

[9] M. M. Negm, "Vector control for induction motor based on minimum variance controller," in *Proc. IEEE-CCECE'97 Conf.*, vol. 2, pp. 761-766, 1997.

[10] T. M. Nasab and M. M. Negm, "Robust performance of induction motor using VSC systems with free chattering," in *Proc. IFAC-IFIP-IMACS Conf. on Control of Industrial Systems*, pp. 223-229, France, 1997.

[11] M. M. Negm, "Torque optimaized speed control of a three phase induction motor," in *Proc. of the IEEE Int. Conf. on Power System Technology, PowerCon '2000*, vol. 1, pp. 67-72, 2000.

[12] M. M. Negm, "SVPWM verification for ANN optimal control of induction motor," in *Proc. of the 37th Int. Universities Power Engineering Conf., UPEC2002*, pp. 488-493, UK, 9-11 Sep. 2002.

[13] National Instruments, *NI 6013/6014 User Manual*, Part Number 323361A-01, Jul. 2002.

[14] Yasuhiko Date, *Servo Motor and Motion Control Using Digital Signal Processors*, Prentice Hall, Englewood Cliffs, 1990.

Mohamed M. Negm was born in Cairo, Egypt, in 1956. He received the B.Sc., M.Sc., and Ph.D. degrees in electrical engineering from Ain-Shams University, Cairo, Egypt in 1979, 1983 and 1990, respectively. During the interval 1985-1989, he was granted a Japanese scholarship at the Department of Electrical Engineering, Faculty of Engineering, Kokkaido University, Japan. Since 2002, he has been with the Department of Electrical Engineering, Faculty of Engineering, Ain-Shams University, Cairo, Egypt, where he is currently a Professor of control of power and electrical machines. His research interest includes interdisciplinary area of optimal preview, VSS, ANN and adaptive control system theories and applications, control of power system, control of electric machines and robotic, control of power electronics devices, advanced process control design, sensorless control and applications of PLC and microprocessors. Professor Negm is a senior member of IEEE.

Mohamed F. Salem was born in Cairo, Egypt, in 1948. He received the B.Sc. and M.Sc. degrees in electrical engineering from Ain-Shams University, Cairo, Egypt in 1971 and 1974, respectively. He received the Ph.D. degree in electrical engineering from Polytechnical Institute, Leningrad, USSR in 1979. During the interval 1980-1984, he was an Associated Professor in the Electrical Department, Ain Shams University. During the interval 1984-1985, he was a visitor Dr. in the Polytechnical Institute, Leningrad, USSR. During the interval 1990-2004, he was a Professor of electrical machines in the Electrical Department, Ain-Shams University. His research interest covers field analysis and design of linear induction machines, linear actuators, induction generators, and their control.

Osama S. Ebrahim was born in Cairo, Egypt, in 1970. He received the B.Sc. and M.Sc. degrees in electrical engineering from Ain-Shams University, Cairo, Egypt in 1994 and 1999, respectively. Since 2004, he has been a Ph.D. staff member in the Electrical Power Department., Ain-Shams University. Cairo, Egypt. His research interest includes analysis and design of electrical machines, modern control theories and their applications, sensorless control of electrical machines, power electronic systems design, and microcontroller applications.